

Orbital-selective correlations and renormalized electronic structure in LiFeAs

Huihang Lin,¹ Rong Yu,^{1,*} Jian-Xin Zhu,^{2,†} and Qimiao Si^{3,‡}

¹*Department of Physics and Beijing Key Laboratory of Opto-electronic Functional Materials and Micro-nano Devices, Renmin University of China, Beijing 100872, China*

²*Theoretical Division and Center for Integrated Nanotechnologies,*

Los Alamos National Laboratory, Los Alamos, New Mexico 87545, USA

³*Department of Physics & Astronomy, Rice Center for Quantum Materials, Rice University, Houston, Texas 77005, USA*

Multiorbital models are important to both the correlation physics and topological behavior of quantum materials. LiFeAs is a prototype iron pnictide suitable for in-depth investigation of this issue. Its electronic structure is strikingly different from the prediction of the noninteracting description. Here, a multiorbital Hubbard model for this compound is studied using a $U(1)$ slave spin theory. We demonstrate a new mechanism for a large change in the size of the Fermi surface, namely, orbital selectivity of the energy-level renormalization cooperating with its counterpart in the quasiparticle spectral weight. Using this effect, we show how the dominating features of the electronic structure in LiFeAs are understood in terms of the local correlations alone. Our results reveal a remarkable degree of universality out of the seemingly complex multiorbital building blocks across a broad range of strongly correlated superconductors.

Introduction. Establishing features that are universal across the different families of strongly correlated systems and identifying properties that are particular to each family are important routes towards elucidating these quantum materials. For iron-based superconductors (FeSCs) [1], an important feature that is of extensive current interest is their multiorbital behavior [2–9]. It has been recognized that electron correlations are strongly orbital dependent in many FeSCs [10–22]. This strong orbital selectivity not only causes large effective mass enhancements [23] and a substantial renormalization of the electronic structure in the normal state [24] but also affects the pairing structure of the superconducting state [25–28]. Previous studies showed that the Hund’s rule coupling between the multiple orbitals plays a crucial role in suppressing the interorbital correlations [10, 13] and pushes the system towards a novel orbital-selective Mott phase (OSMP), in which the iron d_{xy} orbital is Mott localized while other $3d$ orbitals are still itinerant [12]. In experiments, this OSMP can be accessed from a Fermi-liquid-like metallic phase by increasing the temperature [16]. More recently, angular resolved photoemission spectroscopy (ARPES) measurements [29] have implicated an OSMP as a ground state in the iron chalcogenides upon isovalent doping [29], and observed a Fermi surface reconstruction associated with the orbital-selective Mott transition (OSMT): as the OSMP is approached, the hole Fermi pocket with a d_{xy} orbital character at the Brillouin zone (BZ) center vanishes and new features with the itinerant $3z^2 - r^2$ orbital character emerges near the X point. The orbital selective Mott physics is recognized as universal across essentially all the iron chalcogenides [24] and actively interplays with their nematicity and superconductivity [30–34].

In other FeSCs, in particular for iron pnictides, the situation remains open. On general grounds, one may expect that several factors, including the effective or-

bital dependence in the bandwidth and the extent of the kinetic interorbital hybridization as well as the degree of orbital-degeneracy breaking (crystal level splitting) may interplay with the Hund’s coupling and influence the strength of the orbital selectivity. It has been proposed that the orbital selectivity is enhanced when the $3d$ electron occupation number per Fe site is decreased from $n = 6$, the case of the parent compound, towards $n = 5$ [13, 35]. This well accounts for the unusually large effective masses observed in heavily hole doped iron pnictides $A\text{Fe}_2\text{As}_2$ ($A=\text{K, Rb, Cs}$), and prompts a nearby antiferromagnetic ground state in the phase diagram [36] that differs from the one in the parent compounds [5]. For the typical iron pnictides with carrier concentrations close to $n = 6$, there is not yet a clear-cut case for orbital selective correlations.

The 111 iron pnictide LiFeAs presents a promising and pressing case for elucidating the multiorbital correlations of the iron pnictides with broader importance. It superconducts in its pristine form [37, 38], and there is no static magnetic or nematic order in its phase diagram. A recent ARPES study [39] reveals features that are reminiscent of the behavior of the iron chalcogenides. In addition, and particularly notably, its correlation-induced renormalization to the electronic structure near the Fermi energy is especially puzzling.

To put the last feature in a general context, we note that, in general, electron correlations cause mass enhancements, squeezing the bands toward the Fermi level. Without orbital selectivity, the Fermi surface would be unchanged given that the mass enhancement factors are identical in all bands. Surprisingly, in some FeSCs, the observed volume of some Fermi pockets are shrunk compared to that from local density approximation (LDA) calculations; this reflects the opposite (“blue/red”) correlation-induced shifts of the electron and hole bands [40, 41]. In particular for LiFeAs, LDA

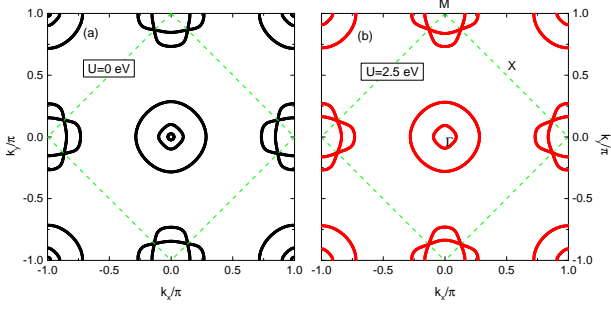


FIG. 1. (Color online) Shrinkage of the Fermi surface induced by local correlations in the model for LiFeAs. The Fermi surfaces are calculated at $U = 0$ (in (a)) and $U = 2.5$ eV (in (b)), respectively. In the correlated case (b), the innermost hole pocket that appears in the $U = 0$ case of (a) disappears and all the other pockets are somewhat reduced.

obtains three hole Fermi pockets centered at Γ point of the BZ. The outermost one has mainly a d_{xy} orbital character, and the inner two are dominated by the $d_{xz/yz}$ orbitals. By contrast, ARPES measurements show that the band giving the innermost hole pocket in LDA is actually below the Fermi level [42–45]. The origin of the the Fermi-pocket reduction is a subject of controversy. In calculations using two-particle self-consistent and/or random phase approximation approaches [46, 47], this reduction is attributed to non-local electron correlations. A more recent study [48] suggests that experimental spectrum observed by ARPES can be fit in terms of a local (*i.e.*, \mathbf{k} -independent) self-energy.

In this letter, we address the orbital selectivity of LiFeAs, with two findings. First, the small As-Fe-As bond angle helps stabilize an OSMF over a broad parameter regime in the ground-state phase diagram. With increasing temperature, the system is driven through an OSMF. Second, we advance a natural but surprising mechanism for a large change in size of the Fermi surface. We demonstrate a new effect, an orbital-selective energy-level renormalization, and show how it cooperates with the orbital dependence in the quasiparticle spectral weight to cause a shrinkage of the Fermi pockets; most drastically, the innermost hole pocket disappears completely (see Fig. 1). Thus, the main features of the electronic structure are captured by the local correlations.

Model and method. We study a five-orbital Hubbard model for LiFeAs. The Hamiltonian reads as

$$H = H_{\text{TB}} + H_{\text{soc}} + H_{\text{int}}. \quad (1)$$

H_{TB} is a five-orbital tight-binding Hamiltonian with tetragonal lattice symmetry [49],

$$H_{\text{TB}} = \frac{1}{2} \sum_{ij\alpha\beta\sigma} t_{ij}^{\alpha\beta} d_{i\alpha\sigma}^\dagger d_{j\beta\sigma} + \sum_{i\alpha\sigma} (\epsilon_\alpha - \mu) d_{i\alpha\sigma}^\dagger d_{i\alpha\sigma}, \quad (2)$$

where $d_{i\alpha\sigma}^\dagger$ creates an electron in orbital α ($\alpha = 1, \dots, 5$

denoting xz , yz , $x^2 - y^2$, xy , and $3z^2 - r^2$ orbitals, respectively) with spin σ at site i , ϵ_α refers to the energy level associated with the crystal field splitting (which is diagonal in the orbital basis), and μ is the chemical potential that fixes the total electron density to 6 per Fe. Importantly, the inter-orbital hopping terms act as a kinetic inter-orbital hybridization [50]. The tight-binding parameters $t_{ij}^{\alpha\beta}$ and ϵ_α for LiFeAs are presented in the Supplemental Material (SM) [51], which are determined by fitting the LDA band structure. As shown in Fig. 1(a) [and also, see below, Fig. 4(a)], this model captures major features of the non-interacting electronic structure of LiFeAs and gives the correct geometry of the LDA Fermi surface. $H_{\text{soc}} = \frac{\lambda_{\text{soc}}^0}{2} \sum_{i\alpha\beta\sigma\sigma'} (\mathbf{L} \cdot \boldsymbol{\tau})_{\alpha\sigma,\beta\sigma'} d_{i\alpha\sigma}^\dagger d_{i\beta\sigma'}$ is an atomic SOC term, where \mathbf{L} denotes the orbital angular momentum operator and $\boldsymbol{\tau}$ refers to the Pauli matrices. λ_{soc}^0 is the (bare) value of the SOC strength without taking into account the effect of electron correlations. We take $\lambda_{\text{soc}}^0 = -30$ meV (see below). The band splitting caused by the SOC is further renormalized by the interactions. The on-site interaction H_{int} reads

$$H_{\text{int}} = \frac{U}{2} \sum_{i,\alpha,\sigma} n_{i\alpha\sigma} n_{i\alpha\bar{\sigma}} + \sum_{i,\alpha<\beta,\sigma} \{ U' n_{i\alpha\sigma} n_{i\beta\bar{\sigma}} + (U' - J_{\text{H}}) n_{i\alpha\sigma} n_{i\beta\sigma} - J_{\text{H}} (d_{i\alpha\sigma}^\dagger d_{i\alpha\bar{\sigma}} d_{i\beta\bar{\sigma}}^\dagger d_{i\beta\sigma} + d_{i\alpha\sigma}^\dagger d_{i\alpha\bar{\sigma}}^\dagger d_{i\beta\sigma} d_{i\beta\bar{\sigma}}) \}, \quad (3)$$

where $n_{i\alpha\sigma} = d_{i\alpha\sigma}^\dagger d_{i\alpha\sigma}$. Here, U , U' , and J_{H} , respectively denote the intra- and inter- orbital repulsion and the Hund's rule coupling, and $U' = U - 2J_{\text{H}}$ is taken [56].

We investigate the correlation effects using a $U(1)$ slave-spin theory [50, 54]. In this approach, we rewrite $d_{i\alpha\sigma}^\dagger = S_{i\alpha\sigma}^+ f_{i\alpha\sigma}^\dagger$, where $S_{i\alpha\sigma}^+$ ($f_{i\alpha\sigma}^\dagger$) is the introduced quantum $S = 1/2$ spin (fermionic spinon) operator to carry the charge (spin) degree of freedom of the electron; the local constraint $S_{i\alpha\sigma}^z = f_{i\alpha\sigma}^\dagger f_{i\alpha\sigma} - \frac{1}{2}$. At the saddle-point level, the constraint is handled via a Lagrange multiplier λ_α and the slave-spin and spinon operators are decomposed so that λ_α and the quasiparticle spectral weight $Z_\alpha \propto |\langle S_\alpha^+ \rangle|^2$ are determined self-consistently [51].

Orbital selectivity in the ground state. We first examine the correlation effects of the model by presenting its ground-state phase diagram in Fig. 2(a). It consists of a metallic phase, an OSMF, and a Mott insulator (MI), with increasing the on-site Coulomb repulsion U . In the metallic phase, there is a crossover at U_{cr} (the red dashed line) from a weakly correlated metal (WCM) to a strongly correlated metal (SCM) with strong orbital selectivity, as shown in Fig. 2(b). In the SCM, the system exhibits bad metal behavior and Z_{xy} is reduced the most. Z_{xy} can be suppressed to zero at U_{OSM} , signaling a transition to an OSMF. Further increasing U the system eventually becomes a MI with electrons in all orbitals localized.

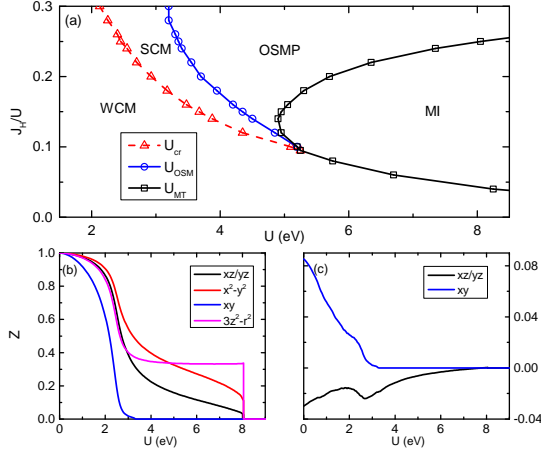


FIG. 2. (Color online) (a): Ground-state phase diagrams of the five-orbital Hubbard models for LiFeAs. MI, OSMP, SCM, and WCM denote the Mott insulator phase, the orbital-selective Mott phase, and the regimes of strongly correlated metal and weakly correlated metal, respectively. U_{cr} refers to a crossover between WCM and SCM. U_{OSM} and U_{MT} denote the critical U values of the orbital-selective Mott transition and the Mott transition, respectively. (b): Evolution of the orbital resolved quasiparticle spectral weights Z with U at $J_H/U = 0.25$ in the model. (c): Effective level energies of the d_{xy} and $d_{xz/yz}$ orbitals with U at $J_H/U = 0.25$.

The phase diagram of LiFeAs differs qualitatively from those of other parent iron pnictides, such as LaOFeAs, where no OSMP exists in the ground-state phase diagram [54]. The stronger orbital selectivity in LiFeAs lies in its smaller As-Fe-As bond angle, which significantly reduces the interorbital hoppings involving the d_{xy} orbital (see SM [51]).

Temperature induced orbital-selective Mott transi-

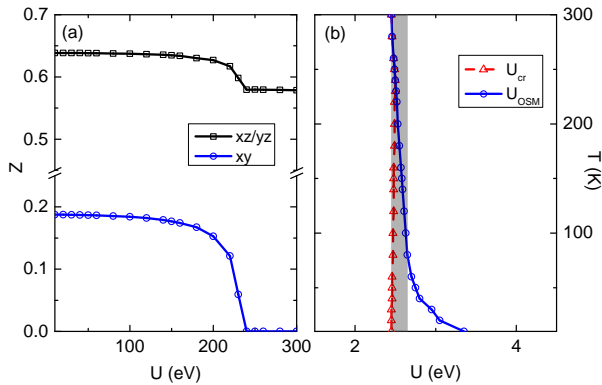


FIG. 3. (Color online) (a): Evolution of the orbital resolved quasiparticle spectral weights with increasing temperature at $J_H/U = 0.25$ and $U = 2.5$ eV for LiFeAs. An OSMT takes place at about 240 K. (b): The thermal phase diagram of the model for LiFeAs at $J_H/U = 0.25$. The shading shows the regime of the estimated U values in LiFeAs.

tion. Given the proximity to the OSMP in the ground state of LiFeAs, we address whether this OSMP can be approached by increasing the temperature. In Fig. 3(a) we show the evolutions of Z_{xy} and $Z_{xz/yz}$ with temperature at $U = 2.5$ eV and $J_H/U = 0.25$. Though $Z_{xz/yz}$ drops slightly and keeps to be finite, Z_{xy} decreases rapidly and vanishes at $T \approx 230$ K, signaling an OSMT. The thermal phase diagram at $J_H/U = 0.25$ is presented in Fig. 3(b). The critical U value for the OSMT, U_{OSM} , decreases with increasing temperature and merges to the crossover line at U_{cr} at high temperatures. By comparing to the experimental mass enhancement factors, we estimate $U \sim 2.4 - 2.7$ eV for $J_H/U = 0.25$ (shaded area in Fig. 4(b)), which results in an OSMT at $T \sim 150 - 250$ K. This is consistent with the temperature evolution observed in a recent ARPES experiment [39].

Renormalization of electronic structure and shrinkage of Fermi pockets. In a single-orbital model, electron correlations modify the electronic structure by renormalizing the bandwidth while keeping the Fermi surface unchanged as a consequence of Luttinger theorem. In a multiorbital model with orbital selectivity, with Z being orbital dependent, the situation is considerably richer.

Our key finding is that the renormalization of the energy levels, ϵ_α , is also orbital-dependent. This warrants the introduction of a second renormalization factor, Z'_α that is also orbital-dependent, specifying the energy-level renormalization:

$$\epsilon'_\alpha = Z'_\alpha \epsilon_\alpha. \quad (4)$$

The renormalized energy level, ϵ'_α , as a function of U is shown in Fig. 2(c). In general, $Z'_\alpha \neq Z_\alpha$, but is a function of all Z_α 's; it is determined consistently from the slave-spin theory.

We now show that the orbital-selective energy-level renormalization, Z'_α , can lead to a shrinkage of the Fermi pockets. We start by specifying the orbital dependence of the quasiparticle weight Z , which differentiates the renormalization of the bands with different orbital characters. This is clearly seen in the calculated bandstructure of LiFeAs in Fig. 4: The bottom of the γ band, with a dominant d_{xy} orbital character, is renormalized from about -0.5 eV to -0.1 eV, with a renormalization factor of about 5; while the bottom of the δ band, with a $d_{xz/yz}$ orbital character, is only renormalized by a factor of about 1.4.

We proceed by focusing on the α , α' , and β bands near the Γ point, which mainly have $d_{xz/yz}$ and d_{xy} orbital characters, respectively. Here, the interorbital hybridization can be neglected. The dispersion can then be expressed as

$$E(\mathbf{k}) \approx Z_\alpha \xi_\alpha(\mathbf{k}) + \epsilon'_\alpha = Z_\alpha [\xi_\alpha(\mathbf{k}) + \epsilon_\alpha] + (Z'_\alpha - Z_\alpha) \epsilon_\alpha, \quad (5)$$

where $\xi_\alpha(\mathbf{k})$ is the Fourier component of the hopping parameter $t_{ij}^{\alpha\alpha}$. For simplicity, we have set the Fermi level

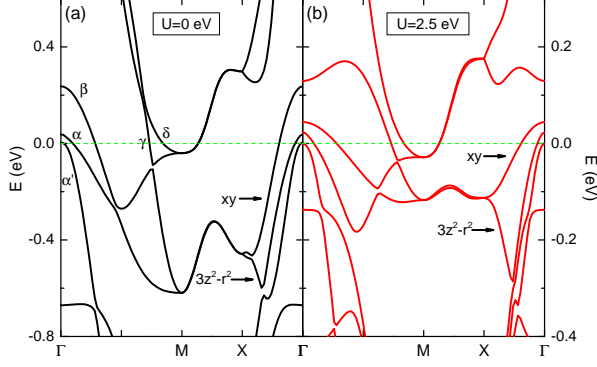


FIG. 4. (Color online) Comparison of the electronic structures in the model for LiFeAs at $U = 0$ (in (a)) and $U = 2.5$ eV (in (b)), respectively, showing a strong renormalization effect. $J_H/U = 0.25$ and $\lambda_{\text{soc}}^0 = -30$ meV are taken in the calculation.

to $E = 0$, and the Fermi surface in the noninteracting limit is defined by $\xi_\alpha(\mathbf{k}) + \epsilon_\alpha = 0$. Clearly, the Fermi surface is un-renormalized if $Z'_\alpha = Z_\alpha$. Importantly, for $Z'_\alpha \neq Z_\alpha$, the Fermi pocket either shrinks or expands depending on the sign of the last term in Eq. (5). For LiFeAs, taking $J_H/U = 0.25$ and $U = 2.5$ eV, we find from Fig. 2 that $Z'_{xy} \approx 0.18 < Z_{xy} \approx 0.19$, $\epsilon_{xy} > 0$, and $Z'_{xz/yz} \approx 0.73 > Z_{xz/yz} \approx 0.63$, $\epsilon_{xz/yz} < 0$. Therefore, according to Eq. (5), the pockets of the α , α' , and β sheets are all reduced in size. The difference between Z_{xy} and Z'_{xy} is relatively small, the Fermi-surface reduction of the β sheet is, correspondingly, relatively small. However, the difference between $Z_{xz/yz}$ and $Z'_{xz/yz}$ is larger. Correspondingly, the shrinkage is considerably stronger for the inner hole pockets. As shown in Fig. 1 and Fig. 4, the innermost α' pocket is completely eliminated. Note that the electron pockets also slightly shrink in a way to fulfill the Luttinger theorem.

Discussions. Several remarks are in order. First, the calculated low-temperature quasiparticle spectral weights $Z_{xy} \approx 0.2$ and $Z_{xz/yz} \approx 0.6$ in the physical regime agree well with the strong orbital dependent mass renormalization factors $(m^*/m_b)_{xy} \sim 4 - 5$ and $(m^*/m_b)_{xz/yz} \sim 1.3 - 2.3$ found in experiments [44]. (We note in passing that the ARPES line-width in LiFeAs may be influenced by the larger k_z -dependence of the xz/yz orbitals than that of the xy orbital [57].) Relatedly, we show that the system undergoes an OSMT at $T \approx 230$ K, which explains the strong reduction of the xy -orbital spectral weight with increasing temperature as observed in ARPES [39]. Both features are to be contrasted with what happens from the non-local correlation effects. The latter would produce a larger renormalization of the quasiparticle weight to the $3d_{xz/yz}$ orbitals than that to the $3d_{xy}$ orbital [46] given that the xz/yz -

orbital-hosting inner hole states have a larger phase space than the xy -orbital-hosting outermost hole Fermi pocket for nested coupling to the electron Fermi pockets via the $(\pi, 0)$ interactions; this is opposite to the ARPES observations of LiFeAs. In addition, the non-local mechanism does not account for the temperature-induced suppression of the $3d_{xy}$ quasiparticle spectral weight.

Second, and importantly, our work advances an entirely new mechanism for the Fermi pocket shrinkage in terms of local, orbital-selective, electron correlations. The key new ingredient is our demonstration of the orbital-selective energy-level renormalization, Z'_α in Eqs. (4,5). The Fermi surface differs from the one in the noninteracting limit only when $Z'_\alpha \neq Z_\alpha$, which is necessarily the case in the presence of orbital selectivity. Our results imply that the dominant effect of electronic-structure-renormalization in LiFeAs, *e.g.* the shrinkage of inner hole pockets, is understood by the local correlations alone. More generally, our work advances a new mechanism for the general phenomenon of “blue/red shifts” [40], namely the differing renormalization of the energy levels and quasiparticle weights, $Z'_\alpha \neq Z_\alpha$.

Third, our results suggest that the electronic structure of the iron pnictides, like their iron chalcogenide counterpart, is predominantly influenced by the local electron correlations. Such correlations provide a starting point to understand the nature of the superconducting state [30, 31, 34]; indeed, our work sets the stage to address the role of short-range interactions in driving the superconductivity of LiFeAs and its derivatives, as has been experimentally implicated [58, 59].

We close the discussion by noting on several additional features. Because of the strong renormalization of the xy orbital, the $3z^2 - r^2$ band along the Γ -X direction is pushed closer to the Fermi level in LiFeAs, as shown in Fig. 4. This serves a particularly convenient diagnostic of strong orbital selectivity [29]. In addition, in strongly correlated electronic topology, multiorbital correlations can play a crucial role for the band inversion and other inherent multi-band behavior. LiFeAs is emerging as a candidate system in which its band topology in the bulk leads to topologically-nontrivial superconductivity on its surface [60]. Given the important role that strong correlations are expected to play in the band inversion of Fe-based systems [61], the orbital-selective correlations we have advanced for LiFeAs set the stage for the much-needed understanding of the topological behavior in LiFeAs. In this connection, we note that, taking into account the renormalization effect on the SOC, the calculated splitting between the α and α' bands is about 20 meV (Fig. 4(b)), which is consistent with the reported value in experiments [42, 45].

Conclusions. We have studied electron correlation effects in a multiorbital Hubbard model for LiFeAs. An orbital-selective Mott phase is found to be stabilized in a broad region of the ground-state phase diagram. We

have identified a new effect of multiorbital correlations, namely orbital selectivity in the energy-level renormalization. This effect interplays with its counterpart in the quasiparticle spectral weight, leading to a natural understanding of the shrinkage in the Fermi pockets and other renormalization of the electronic structure. Our results suggest that the electronic structure of the iron pnictides, like their iron chalcogenide counterpart, is strongly influenced by the local electron correlations. Such correlations underlie the bad-metal normal state observed in many families of strongly correlated superconductors. Our results not only provide the understanding of a striking puzzle in the iron pnictides but also uncover a hidden simplicity in the seeming complexity of the multiorbital superconductors. This implicates a remarkable degree of universality across the iron-based superconductors that is shared with many other families of strongly correlated superconductors.

We thank M. Yi, J. W. Huang, A. Damascelli, R. Day, and P. C. Dai for useful discussions. This work has in part been supported by the National Science Foundation of China Grant No. 11674392, Ministry of Science and Technology of China, National Program on Key Research Project Grant No.2016YFA0300504 and Research Funds of Remnin University of China Grant No. 18XNLG24 (R.Y. and H.L.), and by the U.S. Department of Energy, Office of Science, Basic Energy Sciences, under Award No. DE-SC0018197, the Robert A. Welch Foundation Grant No. C-1411 (Q.S.). Work at Los Alamos was carried out under the auspices of the U.S. DOE NNSA under Contract No. 89233218CNA000001. It was supported by LANL LDRD Program and in part by the Center for Integrated Nanotechnologies, a U.S. DOE BES user facility. Q.S. acknowledges the hospitality of the Aspen Center for Physics, which is supported by NSF grant No. PHY-1607611.

* rong.yu@ruc.edu.cn

† jxzh@lanl.gov

‡ qmsi@rice.edu

- [1] Y. Kamihara, T. Watanabe, M. Hirano, and H. Hosono, “Iron-Based Layered Superconductor $\text{La}[\text{O}_{1-x}\text{F}_x]\text{FeAs}$ ($x = 0.05-0.12$) with $T_c = 26$ K”, *J. Am. Chem. Soc.* **130**, 3296 (2008).
- [2] D. C. Johnston, “The puzzle of high temperature superconductivity in layered iron pnictides and chalcogenides”, *Adv. Phys.* **59**, 803-1061 (2010).
- [3] F. Wang and D.-H. Lee, “The Electron-Pairing Mechanism of Iron-Based Superconductors”, *Science* **332**, 200-204 (2011).
- [4] E. Dagotto, “The Unexpected Properties of Alkali Metal Iron Selenide Superconductors”, *Rev. Mod. Phys.* **85**, 849 (2013).
- [5] P. Dai, “Antiferromagnetic order and spin dynamics in iron-based Superconductors”, *Rev. Mod. Phys.* **87**, 855-896 (2015).
- [6] Q. Si, R. Yu and E. Abrahams, “High Temperature Superconductivity in Iron Pnictides and Chalcogenides”, *Nat. Rev. Mater.* **1**, 16017 (2016).
- [7] P. J. Hirschfeld, “Gap Symmetry and Structure to Reveal the Pairing Mechanism in Fe-based Superconductors”, *Comptes Rendus Physique* **17**, 197 (2016).
- [8] E. Bascones, B. Valenzuela, and M. J. Calderón, “Magnetic interactions in iron superconductors: A review”, *Comptes Rendus Physique* **17**, 36 (2016).
- [9] M. Yi, Y. Zhang, Z.-X. Shen, and D.-H. Lu, “Role of the orbital degree of freedom in iron-based superconductors”, *npj Quant. Mater.* **2**, 57 (2017).
- [10] R. Yu and Q. Si, “Mott Transition in MultiOrbital Models for Iron Pnictides”, *Phys. Rev. B* **84**, 235115 (2011).
- [11] Z. P. Yin, K. Haule, and G. Kotliar, “Magnetism and charge dynamics in iron pnictides”, *Nat. Phys.* **7**, 294(2011).
- [12] R. Yu and Q. Si, “Orbital-Selective Mott Phase in Multiorbital Models for Alkaline Iron Selenides $\text{K}_{1-x}\text{Fe}_{2-y}\text{Se}_2$ ”, *Phys. Rev. Lett.* **110**, 146402 (2013).
- [13] L. de’ Medici, G. Giovannetti, and M. Capone, “Selective Mott Physics as a Key to Iron Superconductors”, *Phys. Rev. Lett.* **112**, 177001 (2014).
- [14] S. Backes, H. O. Jeschke, and R. Valenti, “Microscopic nature of correlations in multiorbital AFe_2As_2 ($A = \text{K, Rb, Cs}$): Hund’s coupling versus Coulomb repulsion”, *Phys. Rev. B* **92**, 195128 (2015).
- [15] N. Patel, A. Nocera, G. Alvarez, A. Moreo, S. Johnston, and E. Dagotto, “Fingerprints of an orbital-selective Mott phase in the block magnetic state of BaFe_2Se_3 ladders”, *Commun. Phys.* **2**, 1 (2019).
- [16] M. Yi, D. H. Lu, R. Yu, S. C. Riggs, J.-H. Chu, B. Lv, Z. K. Liu, M. Lu, Y. T. Cui, M. Hashimoto, S.-K. Mo, Z. Hussain, C. W. Chu, I. R. Fisher, Q. Si, and Z.-X. Shen, “Observation of Temperature-Induced Crossover to an Orbital-Selective Mott Phase in $\text{A}_x\text{Fe}_{2-y}\text{Se}_2$ ($A=\text{K, Rb}$) Superconductors”, *Phys. Rev. Lett.* **110**, 067003 (2013).
- [17] Z. Wang, M. Schmidt, J. Fischer, V. Tsurkan, M. Greger, D. Vollhardt, A. Loidl, and J. Deisenhofer, “Orbital-selective metal-insulator transition and gap formation above T_c in superconducting $\text{Rb}_{1-x}\text{Fe}_{2-y}\text{Se}_2$ ”, *Nat. Commun.* **5**, 3202 (2014).
- [18] X. Ding, Y. Pan, H. Yang, and H.-H. Wen, “Strong and nonmonotonic temperature dependence of Hall coefficient in superconducting $\text{K}_x\text{Fe}_{2-y}\text{Se}_2$ single crystals”, *Phys. Rev. B* **89**, 224515(2014).
- [19] M. Wang, M. Yi, H. Cao, C. de la Cruz, S. K. Mo, Q. Z. Huang, E. B.-Courchesne, P. Dai, D. H. Lee, Z. X. Shen, and R. J. Birgeneau, “Mott localization in a pure stripe antiferromagnet $\text{Rb}_{1-\delta}\text{Fe}_{1.5-\sigma}\text{S}_2$ ”, *Phys. Rev. B* **92**, 121101(R) (2015).
- [20] X. H. Niu, S. D. Chen, J. Jiang, Z. R. Ye, T. L. Yu, D. F. Xu, M. Xu, Y. Feng, Y. J. Yan, B. P. Xie, J. Zhao, D. C. Gu, L. L. Sun, Q. Mao, H. Wang, M. Fang, C. J. Zhang, J. P. Hu, Z. Sun, and D. L. Feng “A unifying phase diagram with correlation-driven superconductor-to-insulator transition for the 122* series of iron chalcogenides”, *Phys. Rev. B* **93**, 054516 (2016).
- [21] M. Hiraishi, K. M. Kojima, H. Okabe, S. Takeshita, A. Koda, R. Kadono, R. Khasanov, S. Iimura, S. Matsushita, H. Hosono, “Magnetism driven by strong electronic correlation in the heavily carrier-doped iron oxypnictide $\text{LaFeAsO}_{0.49}\text{H}_{0.51}$ ”, *arXiv:2004.11547*.

- [22] J. Si, G.-Y. Chen, Q. Li, X. Zhu, H. Yang, and H.-H. Wen, “Unconventional Superconductivity Induced by Suppressing an Iron-Selenium-Based Mott Insulator $\text{CsFe}_{4-x}\text{Se}_4$ ”, *Phys. Rev. X* **10**, 041008 (2020).
- [23] Z.-K. Liu, M. Yi, Y. Zhang, J. Hu, R. Yu, J.-X. Zhu, R.-H. He, Y. L. Chen, M. Hashimoto, R. G. Moore, S.-K. Mo, Z. Hussain, Q. Si, Z. Q. Mao, D. H. Lu, and Z.-X. Shen, “Experimental observation of incoherent-coherent crossover and orbital-dependent band renormalization in iron chalcogenide superconductors”, *Phys. Rev. B* **92**, 235138 (2015).
- [24] M. Yi, Z.-K. Liu, Y. Zhang, R. Yu, J.-X. Zhu, J. J. Lee, R. G. Moore, F. T. Schmitt, W. Li, S. C. Riggs, J.-H. Chu, B. Lv, J. Hu, T. J. Liu, M. Hashimoto, S.-K. Mo, Z. Hussain, Z. Q. Mao, C. W. Chu, I. R. Fisher, Q. Si, Z.-X. Shen, and D. H. Lu, “Observation of universal strong orbital-dependent correlation effects in iron chalcogenides”, *Nat. Commun.* **6**, 7777 (2015).
- [25] R. Yu, J.-X. Zhu, and Q. Si, “Orbital-selective superconductivity, gap anisotropy, and spin resonance excitations in a multiorbital t - J_1 - J_2 model for iron pnictides”, *Phys. Rev. B* **89**, 024509 (2014).
- [26] Z. P. Yin, K. Haule, and G. Kotliar, “Spin dynamics and orbital-antiphase pairing symmetry in iron-based superconductors”, *Nat. Phys.* **10**, 845 (2014).
- [27] T. Ong, P. Coleman, J. Schmalian, “Concealed d-wave pairs in the s^\pm condensate of iron-based superconductors”, *Proc. Nat. Acad. Sci. (USA)* **113**, 5486 (2016).
- [28] E. M. Nica, R. Yu, and Q. Si, “Orbital selective pairing and superconductivity in iron selenides”, *npj Quant. Mater.* **2**, 24 (2017).
- [29] J. Huang, R. Yu, Z. Xu, J. -X. Zhu, Q. Jiang, M. Wang, H. Wu, T. Chen, J. D. Denlinger, S. -K. Mo, M. Hashimoto, G. Gu, P. Dai, J. -H. Chu, D. Lu, Q. Si, R. J. Birgeneau, M. Yi, “Low Temperature Emergence of an Orbital-Selective Mott Phase in $\text{FeTe}_{1-x}\text{Se}_x$ ”, *arXiv:2010.13913* (2020).
- [30] P. O. Sprau, A. Kostin, A. Kreisel, A. E. Böhmer, V. Taufour, P. C. Canfield, S. Mukherjee, P. J. Hirschfeld, B. M. Andersen, J. C. Séamus Davis, “Discovery of orbital-selective Cooper pairing in FeSe ”, *Science* **357**, 75 (2017).
- [31] A. Kostin, P. O. Sprau, A. Kreisel, Yi Xue Chong, A. E. Böhmer, P. C. Canfield, P. J. Hirschfeld, B. M. Andersen, and J. C. Séamus Davis, “Imaging orbital-selective quasiparticles in the Hund’s metal state of FeSe ”, *Nat. Mater.* **17**, 869 (2018).
- [32] L. Fanfarillo, G. Giovannetti, M. Capone, and E. Bascones, “Nematicity at the Hund’s metal crossover in iron superconductors”, *Phys. Rev. B* **95**, 144511 (2017).
- [33] R. Yu, J.-X. Zhu, and Q. Si, “Orbital Selectivity Enhanced by Nematic Order in FeSe ”, *Phys. Rev. Lett.* **121**, (2018).
- [34] H. Hu, R. Yu, E. M. Nica, J.-X. Zhu, and Q. Si, “Orbital-selective superconductivity in the nematic phase of FeSe ”, *Phys. Rev. B* **98**, 220503(R) (2018).
- [35] R. Yu, J.-X. Zhu, and Q. Si, “Orbital-dependent effects of electron correlations in microscopic models for iron-based superconductors”, *Current Opinion in Solid State and Materials Science*, **17**, 65 (2013).
- [36] F. Eilers, K. Grube, D. A. Zocco, T. Wolf, M. Merz, P. Schweiss, R. Heid, R. Eder, R. Yu, J. -X. Zhu, Q. Si, T. Shibauchi, H. Löhneysen, “Quantum criticality in AFe_2As_2 with $A = \text{K, Rb, and Cs}$ suppresses superconductivity”, *Phys. Rev. Lett.* **116**, 237003 (2016).
- [37] X. C. Wang, Q. Q. Liu, Y. X. Lv, W. B. Gao, L. X. Yang, R. C. Yu, F. Y. Li, C. Q. Jin, “The superconductivity at 18 K in LiFeAs system”, *Solid State Commun.* **148**, 538 (2008).
- [38] J. H. Tapp, Z. Tang, B. Lv, K. Sasmal, B. Lorenz, C. W. Chu, and A. M. Guloy “ LiFeAs : An intrinsic FeAs -based superconductor with $T_c=18\text{K}$ ”, *Phys. Rev. B* **78**, 060505(R) (2018).
- [39] H. Miao, Z. P. Yin, S. F. Wu, J. M. Li, J. Ma, B.-Q. Lv, X. P. Wang, T. Qian, P. Richard, L.-Y. Xing, X.-C. Wang, C. Q. Jin, K. Haule, G. Kotliar, and H. Ding, “Orbital-differentiated coherence-incoherence crossover identified by photoemission spectroscopy in LiFeAs ”, *Phys. Rev. B* **94**, 201109 (2016).
- [40] L. Ortenzi, E. Cappelluti, L. Benfatto, and L. Pietronero, “Fermi-surface shrinking and interband coupling in iron-based pnictides”, *Phys. Rev. Lett.* **103**, 046404 (2009).
- [41] G. Lee, H. S. Ji, Y. Kim, C. Kim, K. Haule, G. Kotliar, B. Lee, S. Khim, K. H. Kim, K. S. Kim, K.-S. Kim, and J. H. Shim, “Orbital selective Fermi surface shifts and mechanism of high T_c superconductivity in correlated AFeAs ($A=\text{Li, Na}$)”, *Phys. Rev. Lett.* **109**, 177001 (2012).
- [42] S. V. Borisenko, D. V. Evtushinsky, Z.-H. Liu, I. Morozov, R. Kappenberger, S. Wurmehl, B. Büchner, A. N. Yaresko, T. K. Kim, M. Hoesch, T. Wolf and N. D. Zhigadlo, “Direct observation of spin-orbit coupling in iron-based superconductors”, *Nat. Phys.* **12**, 311 (2016).
- [43] V. Brouet, D. LeBoeuf, P.-H. Lin, J. Mansart, A. Taleb-Ibrahimi, P. Le Fèvre, F. Bertran, A. Forget, and D. Colson, “ARPES view of orbitally resolved quasiparticle lifetimes in iron pnictides”, *Phys. Rev. B* **93**, 085137 (2016).
- [44] J. Fink, J. Nayak, E. D. L. Rienks, J. Bannier, S. Wurmehl, S. Aswartham, I. Morozov, R. Kappenberger, M. A. ElGhazali, L. Craco, H. Rosner, C. Felser, and B. Büchner, “Evidence of hot and cold spots on the Fermi surface of LiFeAs ”, *Phys. Rev. B* **99**, 245156 (2019).
- [45] R. P. Day, G. Levy, M. Michiardi, B. Zwartsenberg, M. Zonno, F. Ji, E. Razzoli, F. Boschini, S. Chi, R. Liang, P. K. Das, I. Vobornik, J. Fujii, W. N. Hardy, D. A. Bonn, I. S. Elfimov, and A. Damascelli, “Influence of Spin-orbit coupling in iron-based superconductors”, *Phys. Rev. Lett.* **121**, 076401 (2018).
- [46] K. Zantout, S. Backes, and R. Valentí, “Effect of nonlocal correlations on the electronic structure of LiFeAs ”, *Phys. Rev. Lett.* **123**, 256401 (2019).
- [47] S. Bhattacharyya, K. Björnson, K. Zantout, D. Steffensen, L. Fanfarillo, A. Kreisel, R. Valentí, B. M. Andersen, and P. J. Hirschfeld, “Non-local correlations in iron pnictides and chalcogenides”, *Phys. Rev. B* **102**, 035109 (2020).
- [48] M. Kim, H. Miao, S. Choi, M. Zingl, A. Georges, and G. Kotliar, “On the Spatial Locality of Electronic Correlations in LiFeAs ”, *arXiv:2009.10577* (2020).
- [49] S. Graser, T. A. Maier, P. J. Hirschfeld, and D. J. Scalapino, “Near-degeneracy of several pairing channels in multiorbital models for the Fe pnictides”, *New J. Phys.* **11**, 025016 (2009).
- [50] R. Yu and Q. Si, “Orbital-selective Mott phase in multiorbital models for iron pnictides and chalcogenides”, *Phys. Rev. B* **96**, 125110 (2017).
- [51] See Supplemental Material [<http://link...>] for details about the tight-binding parameters of the model, the $U(1)$ slave spin theory, and the bond angle and enhanced

- orbital selectivity in LiFeAs, which include Refs. [9, 49, 50, 52–55].
- [52] S. Florens and A. Georges, “Slave-rotor mean-field theories of strongly correlated systems and the Mott transition in finite dimensions”, *Phys. Rev. B* **70**, 035114 (2004).
- [53] G. Kotliar and A. E. Ruckenstein, “New Functional Integral Approach to Strongly Correlated Fermi Systems: The Gutzwiller Approximation as a Saddle Point”, *Phys. Rev. Lett.* **57**, 1362 (1986).
- [54] R. Yu and Q. Si, “ $U(1)$ slave-spin theory and its application to Mott transition in a multiorbital model for iron pnictides”, *Phys. Rev. B* **86**, 085104 (2012).
- [55] M. J. Pitcher, D. R. Parker, P. Adamson, S. J. C. Herkelrath, A. T. Boothroyd, R. M. Ibberson, M. Brunelli and S. J. Clarke, “Structure and superconductivity of LiFeAs”, *Chem. Commun.* **2008**, 5918 (2008).
- [56] C. Castellani, C. R. Natoli, and J. Ranninger, “Magnetic structure of V2O3 in the insulating phase”, *Phys. Rev. B* **18**, 4945 (1978).
- [57] R. P. Day and A. Damascelli, private communications (2020).
- [58] H. Miao, T. Qian, X. Shi, P. Richard, T. K. Kim, M. Hoesch, L. Y. Xing, X.-C. Wang, C.-Q. Jin, J.-P. Hu, and H. Ding, “Observation of strong electron pairing on bands without Fermi surfaces in $\text{LiFe}_{1-x}\text{Co}_x\text{As}$ ”, *Nat. Comm.* **6**, 6056 (2015).
- [59] K. Umezawa, Y. Li, H. Miao, K. Nakayama, Z.-H. Liu, P. Richard, T. Sato, J. B. He, D.-M. Wang, G. F. Chen, H. Ding, T. Takahashi, and S.-C. Wang, “Unconventional Anisotropic s-Wave Superconducting Gaps of the LiFeAs Iron-Pnictide Superconductor”, *Phys. Rev. Lett.* **108**, 037002 (2012).
- [60] P. Zhang, Z. Wang, X. Wu, K. Yaji, Y. Ishida, Y. Kohama, G. Dai, Y. Sun, C. Bareille, K. Kuroda, T. Kondo, K. Okazaki, K. Kindo, X. Wang, C. Jin, J. Hu, R. Thomale, K. Sumida, S. Wu, K. Miyamoto, T. Okuda, H. Ding, G. D. Gu, T. Tamegai, T. Kawakami, M. Sato, and S. Shin, “Multiple topological states in iron-based superconductors”, *Nat. Phys.* **15**, 41 (2019).
- [61] H. Lohani, T. Hazra, A. Ribak, Y. Nitzav, H. Fu, B. Yan, M. Randeria, and A. Kanigel, “Band inversion and topology of the bulk electronic structure in $\text{FeSe}_{0.45}\text{Te}_{0.55}$ ”, *Phys. Rev. B* **101**, 245146 (2020).

SUPPLEMENTAL MATERIAL – ORBITAL-SELECTIVE CORRELATIONS AND RENORMALIZED ELECTRONIC STRUCTURE IN LIFEAS

Details on the tight-binding model

To obtain the tight-binding parameters, we perform LDA calculations for LiFeAs, and fit the LDA bandstructure to the tight-binding Hamiltonian. We use the form of the five-orbital tight-binding Hamiltonian given in Ref. [49]. The tight-binding parameters so derived are listed in Table S1.

The electronic structure of the tight-binding model is shown in Fig. 4(a), which produces the Fermi surface of three hole pockets centered about Γ point and two electron pockets centered about M point, as presented in Fig. 1(a).

To clarify the origin of the enhanced orbital selectivity compared to other parent iron pnictides, we calculated the total density of states (DoS) and the DoS projected to the d_{xy} of the tight-binding model. They are contrasted to those of the tight-binding model for LaOFeAs [49] in Fig. S1. Though the overall DoS of the two models are comparable, the DoS projected to the d_{xy} orbital in the model of LiFeAs has a much narrower bandwidth (~ 2 eV) than in LaOFeAs (~ 3 eV). This indeed suggests a stronger orbital selectivity in LiFeAs; see the main text for a detailed discussion.

Details on the $U(1)$ slave-spin theory

Here we present a brief introduction to the $U(1)$ slave-spin method. For more details, we refer to Refs. [50, 54].

In the $U(1)$ slave-spin formulation, we introduce a quantum $S = 1/2$ spin operator whose XY component ($S_{i\alpha\sigma}^+$) is used to represent the charge degree of freedom of the electron at each site i , in each orbital α and for each spin flavor σ . Correspondingly, we introduce a fermionic “spinon” operator ($f_{i\alpha\sigma}^\dagger$) to carry the spin degree of freedom. The electron creation operator is represented as follows,

$$d_{i\alpha\sigma}^\dagger = S_{i\alpha\sigma}^+ f_{i\alpha\sigma}^\dagger. \quad (\text{S1})$$

This representation has an enlarged Hilbert space compared to the one for the physical d electrons. To restrict the Hilbert space to the physical one, we implement a local constraint,

$$S_{i\alpha\sigma}^z = f_{i\alpha\sigma}^\dagger f_{i\alpha\sigma} - \frac{1}{2}. \quad (\text{S2})$$

This representation contains a $U(1)$ gauge redundancy corresponding to $f_{i\alpha\sigma}^\dagger \rightarrow f_{i\alpha\sigma}^\dagger e^{-i\theta_{i\alpha\sigma}}$ and $S_{i\alpha\sigma}^+ \rightarrow S_{i\alpha\sigma}^+ e^{i\theta_{i\alpha\sigma}}$.

As a result, the slave spins can be used to carry the $U(1)$ -symmetric physical charge degree of freedom, similarly as in the slave-rotor approach [52].

To ensure that the saddle point captures the correct quasiparticle spectral weight in the non-interacting limit (being equal to 1), we define a dressed operator in the Schwinger boson representation of the slave spins (in a way similar to the standard slave-boson theory [53]):

$$\hat{z}_{i\alpha\sigma}^\dagger = P_{i\alpha\sigma}^+ S_{i\alpha\sigma}^+ P_{i\alpha\sigma}^-, \quad (\text{S3})$$

where $P_{i\alpha\sigma}^\pm = 1/\sqrt{1/2 + \delta \pm S_{i\alpha\sigma}^z}$, and δ is an infinitesimal positive number to regulate $P_{i\alpha\sigma}^\pm$. With this construction, Eq. (S1) becomes

$$d_{i\alpha\sigma}^\dagger = \hat{z}_{i\alpha\sigma}^\dagger f_{i\alpha\sigma}^\dagger. \quad (\text{S4})$$

The Hamiltonian given in Eq. (1) of the main text can then be effectively rewritten as

$$\begin{aligned} H = & \frac{1}{2} \sum_{ij\alpha\beta\sigma} t_{ij}^{\alpha\beta} \hat{z}_{i\alpha\sigma}^\dagger \hat{z}_{j\beta\sigma} f_{i\alpha\sigma}^\dagger f_{j\beta\sigma} + \sum_{i\alpha\sigma} (\epsilon_\alpha - \mu) f_{i\alpha\sigma}^\dagger f_{i\alpha\sigma} \\ & - \lambda_{i\alpha\sigma} [f_{i\alpha\sigma}^\dagger f_{i\alpha\sigma} - S_{i\alpha\sigma}^z - 1/2] + H_{\text{int}}^S. \end{aligned} \quad (\text{S5})$$

Here, $\lambda_{i\alpha\sigma}$ is a Lagrange multiplier used to enforce the constraint in Eq. (S2). In addition, H_{int}^S is the interaction Hamiltonian in Eq. (3) of the main text rewritten in the slave-spin representation $H_{\text{int}} \rightarrow H_{\text{int}}^S(\mathbf{S})$ [54]. The quasiparticle spectral weight

$$Z_{i\alpha\sigma} = |\langle \hat{z}_{i\alpha\sigma} \rangle|^2 \propto |\langle S_{i\alpha\sigma}^+ \rangle|^2. \quad (\text{S6})$$

After decomposing the slave spin and spinon operators and treating the constraint on average, we obtain two saddle-point Hamiltonians for the spinons and the slave spins, respectively:

$$H_f^{\text{mf}} = \sum_{k\alpha\beta} \left[\xi_k^{\alpha\beta} \langle \hat{z}_\alpha^\dagger \rangle \langle \hat{z}_\beta \rangle + \delta_{\alpha\beta} (\epsilon_\alpha - \lambda_\alpha - \mu) \right] f_{k\alpha}^\dagger f_{k\beta}, \quad (\text{S7})$$

$$H_S^{\text{mf}} = \sum_{\alpha\beta} \left[Q_{\alpha\beta}^f (\langle \hat{z}_\alpha^\dagger \rangle \hat{z}_\beta + \langle \hat{z}_\beta \rangle \hat{z}_\alpha^\dagger) + \delta_{\alpha\beta} (\lambda_\alpha - \tilde{\mu}_\alpha) S_\alpha^z \right] + H_{\text{int}}^S, \quad (\text{S8})$$

where $\delta_{\alpha\beta}$ is Kronecker's delta function, $\xi_k^{\alpha\beta} = \frac{1}{N} \sum_{ij\sigma} t_{ij}^{\alpha\beta} e^{ik(r_i - r_j)}$, and

$$Q_{\alpha\beta}^f = \sum_{k\sigma} \xi_k^{\alpha\beta} \langle f_{k\alpha\sigma}^\dagger f_{k\beta\sigma} \rangle / 2, \quad (\text{S9})$$

In addition, $\tilde{\mu}_\alpha$ is an effective onsite potential whose definition is given in Ref. [54].

Eqs. (S7) and (S8) represent the main formulation of the $U(1)$ slave-spin approach at the saddle-point level. We study the metal-to-insulator transitions in the paramagnetic phase preserving the translational symmetry. The latter allows us to drop the spin and/or site indices of the slave spins and the Lagrange multiplier λ_α in Eqs. (S7) and (S8). We refer to Refs. [54] and [50] for a detailed derivation of these saddle-point Hamiltonians. At the saddle-point level, Z_α and λ_α are solved self-consistently. For a general multiorbital model three saddle-point solutions can be stabilized: a metallic state with the quasiparticle spectral weight $Z_\alpha > 0$ in all the orbitals, a Mott insulator (MI) with $Z_\alpha = 0$ in all the orbitals with a gapless spinon spectrum, and an OSMP in which $Z_\alpha = 0$ in some orbitals whereas $Z_\alpha > 0$ in the others. The solution of the model for LiFeAs is presented in Fig. 2, along with Fig. S2.

Note that in this approach, the spinon dispersion (along with the dispersion of the physical electrons in the metallic phase) is naturally renormalized by the quasiparticle spectral weights $\sqrt{Z_\alpha Z_\beta}$ and shifted by the effective level energy $\epsilon'_\alpha = \epsilon_\alpha - \lambda_\alpha = Z'_\alpha \epsilon_\alpha$, where Z'_α is a complicated function of Z_α and λ_α in all orbitals. (Here we set the Fermi level at zero energy.)

Bond angle and enhanced orbital selectivity in LiFeAs

As shown in Fig. 2(a) of the main text, the ground-state phase diagram of LiFeAs contains a large regime of OSMP. This differs qualitatively from other parent iron pnictides for which the OSMP was not stabilized in the ground

state [54]; it shows that, in the overall phase diagram of the iron pnictides, the OSMF anchors the SCM phase with a large orbital selectivity. To understand this enhanced orbital selectivity in LiFeAs, we note that its As-Fe-As bond angle is about 103° , which is much smaller than those of other parent iron pnictides ($\gtrsim 110^\circ$), but is similar to that in $\text{Li}_{0.8}\text{Fe}_{0.2}\text{OHFeSe}$ [9, 55]. A smaller bond angle corresponds to an elongated tetragon that significantly reduces the interorbital hoppings involving the d_{xy} orbital because of the in-plane symmetry of this orbital. This is clearly seen by comparing the interorbital hoppings of LiFeAs in Table S1 to those of LaOFeAs in Ref. [49]. Smaller interorbital hoppings result in narrower bandwidth projected to the d_{xy} orbital. As shown in Fig. S1, the projected band of the d_{xy} orbital in LiFeAs is much narrower than that of LaOFeAs though the overall d -orbital bandwidths are comparable between the two cases. This feature leads to the stronger orbital selectivity in LiFeAs.

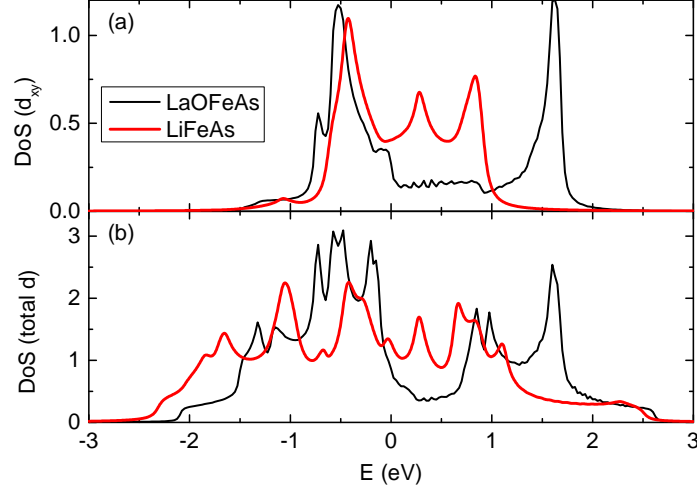


FIG. S1. (Color online) Density of states (DoS) projected onto the d_{xy} (in (a)) and the total d orbitals (in (b)) at $U = 0$ of models for LiFeAs (red curves) and LaOFeAs (black curves), respectively.

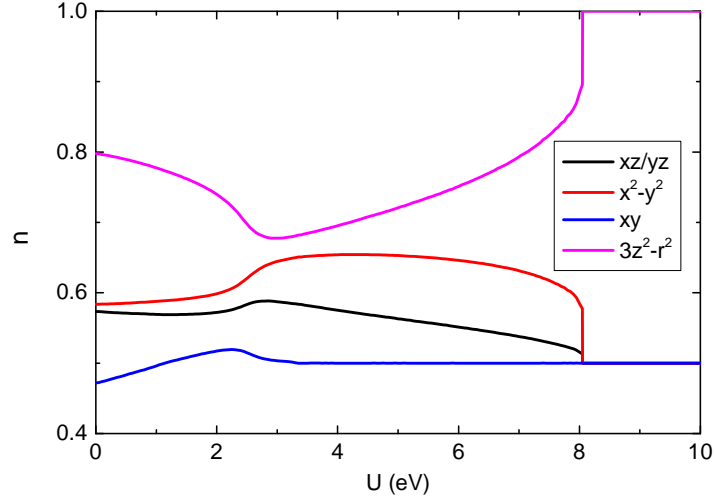


FIG. S2. (Color online) Evolution of the orbital resolved electron occupation number n with U at $J_H/U = 0.25$ for LiFeAs.

	$\alpha = 1$	$\alpha = 2$	$\alpha = 3$	$\alpha = 4$	$\alpha = 5$		
ϵ_α	0.06517	0.06517	-0.38097	0.18026	-0.63628		
$t_\mu^{\alpha\alpha}$	$\mu = x$	$\mu = y$	$\mu = xy$	$\mu = xx$	$\mu = xxy$	$\mu = xyy$	$\mu = xxyy$
$\alpha = 1$	-0.02507	-0.49888	0.24903	0.04834	0.00813	-0.02776	0.04531
$\alpha = 3$	0.42894		-0.01946	-0.01032			
$\alpha = 4$	0.16275		0.13559	-0.00441	-0.05245		-0.03593
$\alpha = 5$	-0.08510			-0.04632	0.01048		-0.00195
$t_\mu^{\alpha\beta}$	$\mu = x$	$\mu = xy$	$\mu = xxy$	$\mu = xxyy$			
$\alpha\beta = 12$		0.19318	-0.05864	0.07046			
$\alpha\beta = 13$	-0.42376	0.07714	0.01353				
$\alpha\beta = 14$	0.03406	-0.02355	-0.00376				
$\alpha\beta = 15$	-0.14608	-0.09700		-0.00683			
$\alpha\beta = 34$			-0.00635				
$\alpha\beta = 35$	-0.26547		0.03472				
$\alpha\beta = 45$		-0.10611		0.03363			

Supplemental Table S1. Tight-binding parameters of the five-orbital model for LiFeAs. Here we use the same notation as in Ref. [49]. The orbital index $\alpha = 1, 2, 3, 4, 5$ correspond to d_{xz} , d_{yz} , $d_{x^2-y^2}$, d_{xy} , and $d_{3z^2-r^2}$ orbitals, respectively. The listed parameters are in eV.